Scale-up of DS-silicon growth process under TMF

N Dropka, T Ervik, F.M. Kiessling

Scale-up of DS-silicon growth process under TMF

N. Dropka, T. Ervik and F.M. Kiessling

Leibniz Institute for Crystal Growth, Max Born Str.2, 12489 Berlin, Germany

natascha.dropka@ikz-berlin.de

Abstract

Despite many research studies of DS-Si growth under TMF at lab scale, transfer of technology to industrial scale is still empirical and limited to low scale-up ratios. To assure safe upscaling, we derived a set of similarity principles for numerical modeling of DS-Si processes in TMF and verified the obtained numerical results with experimental data gained in G1-, G2- and G5-sized furnaces provided with KRIST*MAG*® heater magnet modules. Results pointed out that shared parameters with various exponentiation in various dimensionless numbers hindered accurate upscaling. Nevertheless, with selection of crucial dimensionless numbers and correct definition of the characteristic parameters, the fundamental upscaling from G1 to G5 is feasible.

Key words: directional solidification, simulation, silicon, travelling magnetic field, scale-up

Introduction

A common approach to improve the process economy of directionally solidified silicon (DS-Si) is to scale-up the ingot size. To achieve that, larger ingot cross sections and higher aspect ratios are favorable. In industrial DS-Si, the control of the s/l interface in G4-G6 geometry (G: generation; 4-6: obtained brick number per ingot width for standard wafers 156x156 mm^2) is challenging. Further scaling-up to G7 was demonstrated [1], but due to low crystal quality, this process still hasn't reached industrial maturity. To control morphology and shape of the s/l interface, travelling magnetic fields (TMFs) were proposed and successfully applied [2]. Despite many research studies at lab scale G1, the transfer of technology between different scales is still empirical and limited to low scale-up ratios. In crystal growth practice, the scale up ratio is defined as the ratio of ingot widths i.e. diameters at two scales. Rare fundamental scale-up studies based on 3D modeling were verified in liquid metal set-ups with either small cylindrical $D = H = 14$ cm [3] or small rectangular crucibles $L = W = H = 10$ cm [4], often under isothermal conditions. Bearing in mind: i) the significant difference in heat conductivity and generated latent heat between e.g. GaInSn and Si, and ii) a non-axisymmetric DS-Si furnace geometry, the higher scale-up ratios based on liquid metal experiments easily become speculative.

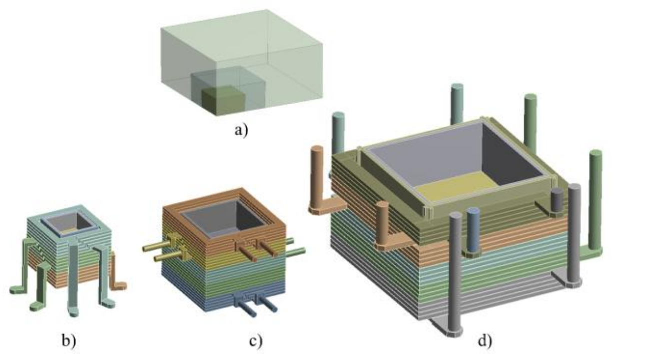

Fig.1: Silicon ingots (a) and crucial parts of G1-, G2- and G5-sized DS-furnaces with KRIST*MAG*® HMMs (b - d).

The aim of this paper was: (i) to derive a set of similarity principles [5] for modeling of DS-Si processes in TMF so that a numerical model can exactly reproduce the coupled transport phenomena and (ii) to verify the obtained numerical results with experimental data from real set-ups. For that purpose, it was necessary to reappraise the definition of dimensionless numbers that are relevant for DS process. Particularly, we studied mc-Si growth in real G1-, G2- and G5-sized furnaces equipped with KRIST*MAG*® heater magnet modules (HMMs) [2, 6] shown in Fig.1.

Model and Methodology

The numerical model described DS-Si growth under TMF. Heat and Lorentz forces F_L were generated by the side KRIST*MAG*® HMM with several heating coils positioned upon each other and supplied with a combination of ac and dc. Supplementary heat originated from top and bottom resistance heaters in meander-form. The transport phenomena taking place in G1-, G2- and G5- sized furnaces were governed by the equations of continuity, Navier Stokes, energy and induction together with the Ohms law given elsewhere [7]. Due to the complexity of 3D models, we solved them stepwise, performing global 3D simulations for each furnace neglecting Si melt flow and local 3D simulations for Si flows driven by buoyancy and TMF. The global CFD analysis provided thermal boundary conditions (BCs) for the local simulations. Furthermore, the global 3D electro-magnetic (EM) analysis provided the Lorentz force density fields for the local simulations. Pure buoyancy driven melt flows were used for initiation of the magnetic driven flows and as a benchmark.

The 3D CFD and EM simulations were performed using the commercial software ANSYS CFX 14.0 and Ansys Emag.

The scale-up was discussed using dimensionless quantities such as Reynolds *Re* (1), Grashof *Gr* (2), Stefan *Ste* (3), magnetic forcing *F* (4), magnetic Reynolds Re_m (5) and Shielding *S* (6) number. Skin depth δ of TMF was defined in (7). The notation corresponded to the ones in [11].

$$Re = \frac{u \cdot L^* \cdot \rho}{\mu};\ Gr = \frac{\beta \cdot g \cdot \Delta T_{x,y} \cdot L^{*3}}{\nu^2};\ Ste = \frac{\lambda_S \left(\frac{\Delta T}{\Delta z}\right)_s - \lambda_L \left(\frac{\Delta T}{\Delta z}\right)_l}{r_{growth} \cdot \rho_S \cdot \Delta H_{sl}};\ F = \frac{F_L \cdot L^{*3} \cdot \rho}{\mu^2}; \tag{1-7}$$

$$Re_m = \mu_0 \cdot \sigma_{el} \cdot u \cdot L^*;\ S = 2\left(\frac{L^*}{\delta}\right)^2;\ \delta = \left(\mu_r \cdot \mu_0 \cdot \sigma_{el} \cdot \pi \cdot f\right)^{-0.5}$$

The characteristic length L^* was defined individually for each transport phenomenon, e.g. in case of flow $L^* = (V_l)^{1/3}$ while for thermal and EM simulations, half ingot width was used $L^* = L/2$. The symbols V_l, r_{growth} and $\Delta T_{x,y}$ corresponded to the melt volume, the crystal growth rate and the horizontal temperature difference, respectively.

Tab.1: TMF parameters used in verification experiments.

size	f_1; f_2 [Hz]	$\Delta\phi_1$; $\Delta\phi_2$ [°]	I_1 / I_2 [1]	F_L direction
G1	20; 200	-90; +90	2.3	down
G2	20; 200	+90; -90	10	up
G5	20; 250	-90; +90	10	down

In definition of *Re*, Re_m and *F*, maximal values of melt velocity *u* and Lorentz force density F_L were used. The crystal growth was performed in *z*-direction.

The influence of ingot size on F_L was studied numerically in G1-, G2- and G5-sized furnaces in the wide range of EM parameters: frequency f = 10 - 600 Hz, phase shift $\Delta\phi$ = 0° ± 110° and ac amplitude I_o = 0 - 500 A.

Verification experiments were performed in G1-, G2- and G5-sized furnaces loaded with 14 kg, 75 kg and 640 kg Si respectively. Corresponding ingot aspect ratios *L / H* were 1.7, 1.9 and 2.1. Average experimental growth rate was ca. r_{growth} = 1 cm/h. EM parameters of double frequency 2f-TMF that were used in experiments are given in Tab. 1. Double frequency 2f-TMFs were used in order to protect crucible coatings by shifting the maximal velocities towards the melt bulk [8].

Results and Discussions

The influence of ingot size on F_L magnitude, direction, and distribution in the melt is given in Fig. 2 and Fig. 3.

The results showed that the magnitude of F_L at all scales depends nearly linearly on frequency, quadratically on ac magnitude and exhibits a maximum at phase shift $\Delta\phi$ = 0° (Fig. 2). The reversal of F_L maxima between G1- and G2-case (Fig. 2b) was a consequence of their unequal number of heating coils. For the same number of heating coils, the reversal didn't appear, i.e. the highest F_L maximum was obtained in G1-case followed by G2- and G5-cases, respectively. For the same EM parameters, upscaling of the melt decreased the F_L magnitude significantly. Conversely e.g. to achieve the same magnitude of F_L at higher scales by constant f and $\Delta\phi$, ac has to increase.

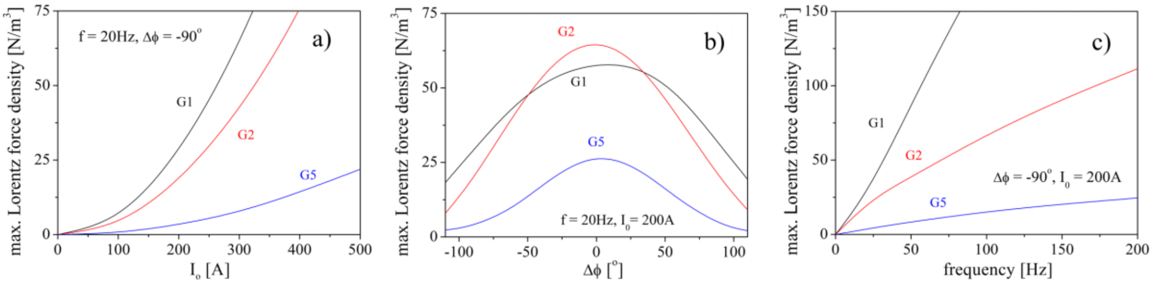

Fig. 2: Maximal Lorentz force density in G1-, G2- and G5-sized furnaces as a function of: a) ac amplitude, b) phase shift and c) frequency.

Considering F_L direction and spatial distribution at all scales, our findings revealed the crucial role of frequency. With an increase in frequency, the slope of F_L vectors decreased (Fig.3a,d). Moreover, by the increase of frequency from e.g. 10 to 50 Hz, TMF penetration depth δ decreased from 145 mm to 65 mm. Full penetration of G5 melt i.e. $\delta = L^*$ was achieved for $f \leq 1.2$ Hz. Nevertheless, very low frequencies are not feasible for practical applications due to ac demand above the thermal requirements of the process. For the same EM parameters, the slope of F_L vectors remained the same during upscaling (Fig.3a-c). The small discrepancy observed at the bottom region originated from the axially off centered melt position relative to the HMM in G2 and G5 furnaces. If common three-phase ac (f = 50 Hz, $\Delta\phi$ = -120°)

was used for generation of TMF, F_L vectors would have axially non-uniform low slope and magnitude. For practical application, TMF has to be accurately adjusted with a time to both: cooling program and to the position of s/l interface relative to the heaters that is a challenge. Therefore, ac with lower frequency (e.g. $f \leq 20$ Hz) and negative phase shift of ca. $\Delta\phi = -90°$ is a better choice for interface shaping due to higher δ, higher F_L slope and relatively uniform axial magnitude distribution.

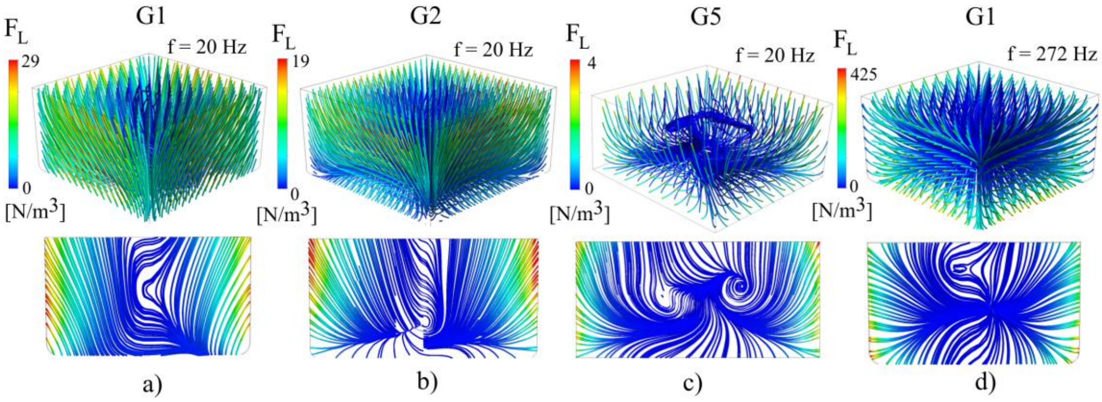

Fig. 3: Lorentz force density streamlines in Si melt at various scales for: a-c) $f = 20$ Hz, $\Delta\phi = -90°$ and $I_0 = 200$ A, d) $f = 272$ Hz, $\Delta\phi = -90°$ and $I_0 = 200$ A.

If scale-up from G1- to G5-size was analyzed using dimensionless magnetic numbers, the following results were obtained: for constant $f = 20$ Hz, Shielding number S increased as expected from $S_{G1} = 2.4$ to $S_{G2} = 7.0$ and $S_{G5} = 32.9$. According to the similarity theory, the same S values assure similar penetration behavior of TMF at various scales. In our case $S_{G5} = 32.9$ in G5 furnace will be also obtained in G1 furnace if f increases to $f = 272$ Hz. Nevertheless, such increased frequency brought significant loss in the slope of F_L vectors (Fig.3a,d) that is crucial for interface shaping. Therefore, Shielding number S seems to be less relevant for DS-Si growth if the goal of TMF application is to provide slightly convex s/l interface shape. Further on, magnetic forcing F increased by upscaling even if EM parameters were kept constant i.e. if F_L decreased. For the cases shown in Fig.3a-c, F had a values of $F_{G1} = 1.36 \cdot 10^8$, $F_{G2} = 4.46 \cdot 10^8$ and $F_{G5} = 8.36 \cdot 10^8$, respectively. For preserving the F value constant by upscaling from G1- to G5-size, Lorentz force density F_L should decrease 50.6 times down to the negligible value of $F_L = 0.57$ N/m^3. Obviously magnetic forcing F alone is not able to describe magnetic similarity.

The s/l interface shapes obtained in verification experiments in G1-, G2- and G5-sized furnaces in form of Lateral Photovoltage Scanning (LPS) images [9] of ingot vertical cuts are shown in Fig.4. As already presented in our previous papers e.g. [7, 8, 10], upwards directed TMF promoted s/l interface concavity (Fig.4b), while downwards directed TMF promoted convex interface (Fig.4a, c).

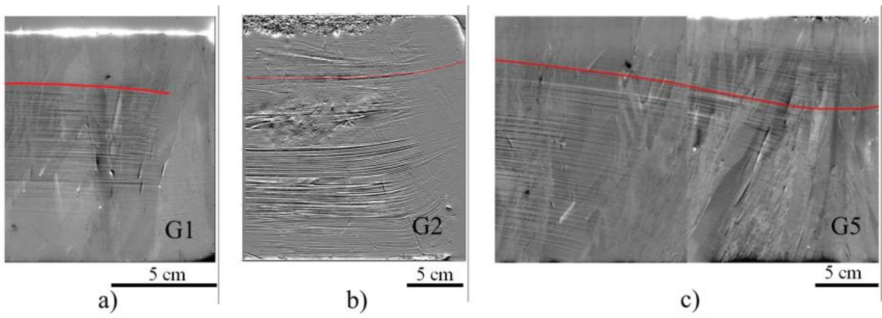

Fig. 4: LPS images of G1- (a), G2- (b) and G5-sized (c) partial (right-half) vertical cuts of ingots grown in downwards (a, c) and upwards (b) 2f-TMFs; interface curvature and crucible right side wall were marked red and black, respectively; image (c) was reprinted from [10] with permission of Elsevier.

Similar temperature fields and interface deflections were obtained in our 3D simulations. An example of simulated temperature and velocity distributions obtained during Si growth in G2-sized furnace exposed to upwards 2f-TMF is shown in Fig.5. The Lorentz force density streamlines in the melt corresponded to EM parameters given in Tab.1. The Lorentz force density maximum was located at the middle of the crucible side walls near s/l interface (Fig.5a). The melt flow was in laminar regime with a velocity maximum located at the melt diagonals near the free surface (Fig.5c). The flow exhibited a complex 3D multi-vortex pattern with dominantly upward directed velocities at the melt side peripheries. Particularly the velocities in this peripheral region determined the concave interface shape. In downwards directed TMF in G1 and G5 case studies, again the 3D multi-vortex velocity pattern was obtained with dominantly downward directed velocities near the three-phase junction that induced convex interface [10]. In all considered cases, laminar regime was obtained. Simulation results showed that in upscaled cases, stronger F_L were needed to counteract buoyancy force and flatten the interface.

In dimensionless numbers, upscaled G2 case with ca. half crystallized Si was characterized by $F = 9.6 \cdot 10^7$, $Re = 1.04 \cdot 10^4$, $Gr = 1.75 \cdot 10^8$, $Re_m = 4.16 \cdot 10^{-3}$ and $Ste = 2.21 \cdot 10^{-1}$. At G5 scale with 20% crystallized Si, dimensionless numbers reached following values: $F = 1.9 \cdot 10^9$, $Re = 1.41 \cdot 10^4$, $Gr = 1.78 \cdot 10^9$, $Re_m = 5.23 \cdot 10^{-3}$ and $Ste = 7.5 \cdot 10^{-2}$. Obviously, neither of these numbers, if considered separately was able to relate F_L with buoyancy force that is crucial for interface shaping. As already shown for VGF-GaAs growth [11], a combined dimensionless number $F \cdot Gr^{-1} \cdot Ste^{-1}$ contained all relevant variables for crystal growth in TMF: temperature gradients, growth rate and Lorentz force density. If the aim of TMF application is exclusively the interface shaping, then only axial F_L component in the vicinity of three-phase junction should be used for the calculation of F. Please note that L^* didn't appear in this combined number. Nevertheless, the increase of ingot size was accounted indirectly by the increased ∇T and needed F_L to compensate the buoyancy force.

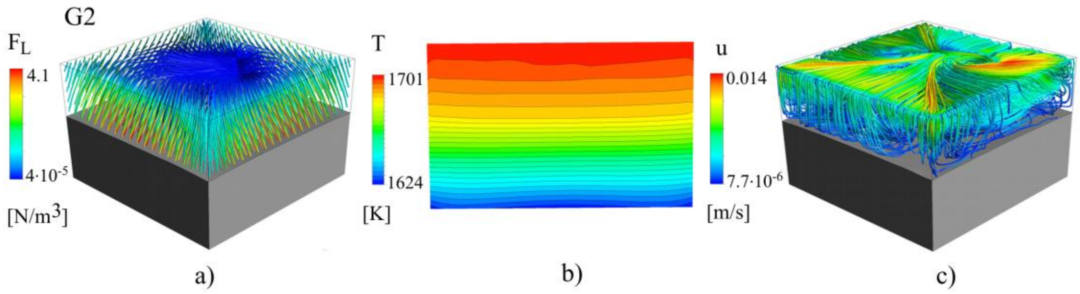

Fig. 5: Simulation results for Si growth in G2-sized furnace exposed to upwards 2f-TMF defined in Tab.1: a) Lorentz force density streamlines in the melt, b) temperature distribution in Si in vertical mid plane, c) velocity streamlines in the melt.

Conclusions

Our 3D simulation results showed that TMF, if its EM parameters were carefully selected is a very promising tool for the control of s/l interface shape in DS-Si growth at various scales. Particularly, we studied scale-up in G1-, G2- and G5-sized furnaces that are using KRIST*MAG*® technology for the generation of TMF. Based on the simulation findings, we proposed a method for the theoretical, i.e. numerical scale-up using a combination of dimensionless numbers Grashof *Gr*, Stephan *Ste* and magnetic forcing number *F*. Obtained numerical results were in good agreement with experiments.

Acknowledgment

Experimental support of Ch. Frank-Rotsch, R. Menzel and D. Linke during the growth of G2 crystal and T. Turschner and S. Kayser for providing LPS images is gratefully acknowledged.

References

[1] http://www.ldksolar.com/pro_ingot_overview.php
[2] P. Rudolph (2008), J. Cryst. Growth 310, 1298-1306
[3] I. Grants, C. Zhang, S. Eckert, G. Gerbeth (2008), J. Fluid Mech. 616, 135-152
[4] K. Dadzis (2012), Modeling of directional solidification of multicrystalline silicon in a traveling magnetic field, PhD thesis, TU Bergakademie Freiberg
[5] S.J. Kline (1986), Similitude and Approximation Theory, Springer-Verlag, New York
[6] P. Lange, M. Ziem, P. Rudolph (2009), Patent DE 10 2009 045 680A1
[7] N. Dropka, Ch. Frank-Rotsch, P. Rudolph (2013), J. Cryst. Growth 365, 64-72
[8] N. Dropka, W. Miller, U. Rehse, P. Rudolph, F. Buellesfeld, U. Sahr, O. Klein, D. Reinhardt (2011), J. Cryst. Growth 318, 275-279
[9] N.V. Abrosimov, A. Ludge, H. Riemann, W. Schroder (2002) J. Cryst. Growth 237-239, 356-360
[10] Ch. Kudla, A.T. Blumenau, F. Büllesfeld, N. Dropka, Ch. Frank-Rotsch, F. Kiessling, O. Klein, P. Lange, W. Miller, U. Rehse, U. Sahr, M. Schellhorn, G. Weidemann, M. Ziem, G. Bethin, R. Fornari, M. Müller, J. Sprekels, V. Trautmann, P. Rudolph (2013), J. Cryst. Growth 365, 54 -58
[11] N. Dropka, Ch.Frank-Rotsch (2013), J. Cryst. Growth 367, 1-7